Conformational and Dynamic Changes of *Yersinia* Protein Tyrosine Phosphatase Induced by Ligand Binding and Active Site Mutation and Revealed by H/D Exchange and Electrospray Ionization Fourier Transform Ion Cyclotron Resonance Mass Spectrometry†

Fang Wang,‡ Weiqun Li,§ Mark R. Emmett,‡ Christopher L. Hendrickson,‡ and Alan G. Marshall*,§

Center for Interdisciplinary Magnetic Resonance, National High Magnetic Field Laboratory, and Department of Chemistry, 1800 East Paul Dirac Drive, Florida State University, Tallahassee, Florida 32310

Yan-Ling Zhang, Li Wu, and Zhong-Yin Zhang*

Departments of Molecular Pharmacology and Biochemistry, Albert Einstein College of Medicine, 1300 Morris Park Avenue, Bronx, New York 10461

Received June 22, 1998; Revised Manuscript Received August 12, 1998

ABSTRACT: Protein tyrosine phosphatases (PTPase) play important roles in the intracellular signal transduction pathways that regulate cell transformation, growth, and proliferation. Here, solvent accessibility is determined for backbone amide protons from various segments of wild-type *Yersinia* PTPase in the presence or absence of 220 μM vanadate, a competitive inhibitor, as well as an active site mutant in which the essential cysteine 403 has been replaced by serine (C403S). The method consists of solution-phase H/D exchange, followed by pepsin digestion, high-performance liquid chromatography, and electrospray ionization high-field (9.4 T) Fourier transform ion cyclotron resonance mass spectrometry. Proteolytic segments spanning ~93.5% of the primary sequence are analyzed. Binding of vanadate reduces the H/D exchange rate throughout the protein, both for the WpD loop and for numerous other residues that are shielded when that loop is pulled down over the active site on binding of the inhibitor. The single active site C403S mutation reduces solvent access to the WpD loop itself, but opens up the structure in several other segments. Although the 3D structure of the ligand-bound C403S mutant is similar to that of the wild-type PTPase, and the C403S mutant and the wild-type enzyme display similar affinities for vanadate, the thermodynamics for binding of vanadate is different for the two proteins. Collectively, these results establish the flexibility of the WpD loop (previously inferred by comparing PTPase X-ray single-cyrstal diffraction structures in the presence and absence of a tungstate inhibitor), as well as several other signficant changes in segment exposure and/or flexibility that are not evident from X-ray structures.

Protein tyrosine phosphatases (PTPases)[1] catalyze the hydrolysis of the phosphate moiety of phosphotyrosine (pTyr) and play important roles in the intracellular signal transduction pathways that regulate cell transformation, growth, and proliferation. The PTPase superfamily presently comprises approximately 100 enzymes, including tyrosine-specific, dual specificity (cleaves pTyr and pSer/pThr), and low molecular weight phosphatases (*1*). The hallmark of this family of enzymes requires the presence of the PTPase signature motif, (H/V)**C**X_5**R**(S/T), housed within the catalytic domain. The PTPase-catalyzed reaction proceeds through a double-displacement mechanism in which the phosphoryl group from the pTyr in a substrate is first transferred to the active site Cys residue within the PTPase signature motif leading to the formation of a cysteinyl phosphate intermediate that is subsequently hydrolyzed by water (*2*, *3*). To facilitate substrate turnover, PTPases also employ an invariant Asp residue acting as a general acid/base catalyst (*4*).

Yersinia, the causative bacterium of bubonic plague and other enteric diseases, secretes an active PTPase (*5*), Yop51, which enters and suppresses host immune cells (*6*, *7*). The *Yersinia* PTPase has been extensively characterized both mechanistically and structurally (*1*). The crystal structures of the unliganded and various oxyanion-bound forms of the *Yersinia* PTPase have been solved (*8*, *9*). The phosphoryl-

†Supported by the NSF High-Field FT-ICR Mass Spectrometry Facility (CHE-94-13008), NIH (GM-31683 and CA 69202), Florida State University, and National High Magnetic Field Laboratory in Tallahassee, FL.

* Address correspondence to Dr. Alan G. Marshall, telephone, (850) 644-0529; fax, (850) 644-1366; e-mail, marshall@magnet.fsu.edu; and Dr. Zhong-Yin Zhang, telephone, (718) 430-4288; fax, (718) 430-8922; e-mail, zyzhang@aecom.yu.edu.

‡ Center for Interdisciplinary Magnetic Resonance, National High Magnetic Field Laboratory.

§ Department of Chemistry, Florida State University.

[1] Abbreviations: PTPase, protein tyrosine phosphatase; NMR, nuclear magnetic resonance; FT-ICR MS, Fourier transform ion cyclotron resonance mass spectrometry; HSQC, ^{1}H,^{15}N-heteronuclear single quantum correlation spectroscopy; ESI, electrospray ionization; HPLC, high-performance liquid chromatography; LC/MS, reversed-phase HPLC coupled to an FT-ICR mass spectrometer; IRMPD, infrared multiphoton dissociation; SWIFT, stored waveform inverse Fourier transform; MEM, maximum entropy method.

10.1021/bi981481q CCC: $15.00
Published on Web 10/16/1998

binding pocket is primarily composed of the PTPase signature motif including the nucleophilic Cys403. The general acid/base Asp356 (*4*) is located in a flexible surface loop (the WpD loop, residues 350−360) in the vicinity of the active site. However, in the unliganded *Yersinia* PTPase structure, the WpD loop is observed in an open conformation such that Asp356 is more than 10 Å away from the phosphate-binding site. Upon oxyanion or substrate binding, the WpD loop adopts a closed conformation, covers the active site like a "flap", and positions the carboxyl group of Asp356 close to the leaving group oxygen of a substrate. Thus, it is clear that the loop must be in its closed form to dispose the general acid/base in a catalytically competent position. Following the chemical step, the loop must reopen to allow the release of the phosphate product.

The conformational changes and dynamic properties of the WpD loop have been investigated by time-resolved fluorescence anisotropy, steady-state fluorescence, and ultraviolet resonance Raman spectroscopies (*10*, *11*). Results from those solution studies indicate that, in the absence of ligand, the WpD loop exists as an equilibrium mixture of almost equal populations of the closed and open conformations, and the *Yersinia* PTPase alternates rapidly between an open WpD loop and a closed WpD loop form with a rate constant of 2.6×10^8 s^{-1}. Upon ligand binding, the closed conformation is preferentially stabilized by the bound ligand. Surprisingly, the WpD loop in the catalytically inactive C403S mutant PTPase adopts a closed conformation with much reduced dynamics.

Protein hydrogen exchange has become a powerful tool to probe the higher-order structure and dynamics of proteins (*12*, *13*). Amide hydrogen/deuterium (H/D) exchange rates for small soluble proteins can be determined by high-resolution multidimensional nuclear magnetic resonance (NMR) spectroscopy (*14*). Mass spectrometry has become increasingly popular for measurement of hydrogen/deuterium exchange rates. Deuterium exchange, combined with mass spectrometric proteolytic mapping, permits segment-specific identification of solvent-accessible exchange sites (*15*−*18*). The ultrahigh mass resolving power of Fourier transform ion cyclotron resonance mass spectrometry (FT-ICR MS) (*19*−*24*) makes it optimal for H/D exchange analysis because isotopic distributions may be resolved in all but very large proteins (*25*−*28*). Furthernore, the upper mass limit for FT-ICR MS may be extended by almost an order of magnitude by double depletion of ^{13}C and ^{15}N proteins (*29*).

In this paper, we further examine the dynamic and conformational properties of both the wild type and the C403S mutant *Yersinia* PTPases by monitoring backbone amide hydrogen exchange combined with electrospray ionization (ESI) FT-ICR MS. Although the WpD loop motion has been observed for the tyrosine-specific phosphatases, it is not clear whether a similar loop motion also occurs in the dual specificity and low molecular weight phosphatases. It is expected that the amide protons in the WpD loop will be protected from exchange in the closed conformation. Thus, a second goal is to establish if vanadate binding can protect the WpD loop amide from exchange and whether such protection can be detected by ESI−FT-ICR MS. If the answers to both questions are positive, one can then apply these techniques to probe loop motions in the dual specificity and the low molecular weight phosphatases. We find that deuterium incorporation in several loop regions (including the WpD loop region) in the vanadate-complexed wild-type PTPase, as well as ligand-free and bound C403S mutant, differs significantly from that for wild-type unliganded PTPase. Although the wild type and the C403S mutant *Yersinia* PTPases possess similar affinities for vanadate, the enthalpic and entropic contributions to binding differ significantly. H/D exchange combined with ESI−FT-ICR mass analysis exposes dramatic differences in solvent accessibility that are not apparent from X-ray crystal structures.

MATERIALS AND METHODS

Enzyme Preparation. A recombinant *Yersinia* PTPase (Yop51*/Δ162) that lacked the N-terminal 162 amino acids was used in this study. Yop51*/Δ162 encompasses the entire catalytic domain of the native *Yersinia* PTPase and contains a C235R point mutation that dramatically increases its expression level in *Escherichia coli* (*30*). Yop51*/Δ162 is kinetically indistinguishable from the full-length native enzyme and is the form used for all X-ray structural studies. We henceforth refer to Yop51*/Δ162 as wild-type *Yersinia* PTPase. Homogeneous recombinant *Yersinia* PTPase was expressed and purified as previously described (*30*). Site-directed mutagenesis of residue Cys403 of the *Yersinia* PTPase to Ser was carried out by use of the Muta-Gene in vitro mutagenesis kit from Bio-Rad (*11*). The expression and preparation of homogeneous recombinant C403S mutant PTPase were performed as previously described (*11*).

Materials. Pepsin was obtained from Worthington, Co. (Lakewood, NJ) and D_2O (99.9 atom % D) from Aldrich Chemical Co. (Milwaukee, WI). All other chemicals and reagents were of the highest grade commercially available. The procedure for the preparation of the stock solution of sodium orthovanadate has been described previously (*31*).

Hydrogen Exchange. H/D exchange was initiated by 20-fold dilution, namely, by adding 20 μL of a 400 μM solution of wild-type PTPase or C403S mutant PTPase in 50 mM 3,3-dimethylglutarate buffer, pH 6.5, 0.15 M sodium chloride, in the presence or absence of 2.5 mM vanadate, to 380 μL of corresponding 99.9 atom % D_2O in the presence or absence of 100 μM vanadate. Solutions were maintained at 25 °C in a water bath and incubated for various H/D exchange periods. At appropriate intervals, aliquots of the PTPase solution were quenched by the addition of an equal volume of 0.5 M phosphate buffer, pH 2.2, and immediately frozen in liquid N_2. The samples were stored at −70 °C until analysis.

Pepsin Digestion. The deuterated protein was thawed on ice. A 90-μL aliquot of deuterated protein solution was added to 6 μL of 80 μM pepsin in 0.5 M phosphate buffer, pH 2.2, injected onto a 20-μL injection loop, and allowed to digest for 3 min at 0 °C in the loop prior to HPLC analysis.

LC-ESI FT-ICR MS Analysis of the Deuterated PTPase and its Peptic Digest Peptides. The extent of deuterium incorporation into PTPase and localization was determined by LC-ESI FT-ICR MS analysis. Acetonitrile gradients at 30 μL/min were generated with a Shimadzu HPLC equipped with two LC-10AD pumps. Solvent A was 94.5% H_2O containing 5% acetonitrile and 0.5% formic acid (pH 2.3), and solvent B was 80% acetonitrile containing 19.5% H_2O and 0.5% formic acid. A low-volume static mixing tee was

used to minimize the delay period for HPLC. The solvent precooling coil, static mixing tee, Rheodyne injector, and column were immersed in an ice bath (0 °C) to minimize back exchange with HPLC solvents. Aliquots (5 μL) of the exchanged and quenched protein solution or aliquots (20 μL) of the pepsin digests were loaded onto a Vydac 1.0 × 50 mm C_4 or C_8 column, respectively. After being desalted at 5% B for 2 min, the protein eluted at ~4.3 min with a 2-min 5%−90% B gradient, and the peptic peptides eluted between 4 and 9 min with a 7-min 5%−50% B gradient. The column effluent (30 μL/min) was delivered directly to the mass spectrometry without flow split.

To account for deuterium gain or loss under quenched conditions, we prepared two control samples (*15*). A "zero-deuteration" control was prepared by diluting the protiated protein solution directly into a 1:1 (v/v) mixture of deuterated buffer and quenching buffer. A "full-deuteration" control was prepared by incubating PTPase in deuterated buffer, pH meter reading 6.1, at 55 °C for 4 h, followed by incubation in deuterated solution, pH meter reading 2.5, at 55 °C for an additional 4 h (see Results).

Identification of Proteolytic Segments. PTPase was digested with pepsin (~2:1 substrate/enzyme mole ratio) at pH meter reading 2.2 and at 0 °C for 3 min, then subjected to HPLC analysis. The HPLC fractions were collected and analyzed by off-line ESI−FT-ICR MS with melittin as an internal mass calibration standard. Mass resolving power, $m/\Delta m_{50\%}$ (in which $\Delta m_{50\%}$ is the mass domain peak full width at half-maximum peak height), ranged between 50 000 and 120 000, depending on the peptide mass-to-charge ratio, (m/z). When infrared multiphoton dissociation (IRMPD) (*32*) was carried out, ions of a given m/z ratio were isolated selectively by stored waveform inverse Fourier transform (SWIFT) broadband ejection of ions of all other m/z values (*33*, *34*), and the isolated parent ions were fragmented by infrared irradiation at 30−40 W for 0.4−1 s.

Mass Spectrometry. Mass analyses were performed with a home-built FT-ICR mass spectrometer, based on a shielded 9.4 T superconductive magnet, and equipped with a home-built external electrospray interface described elsewhere (*27*, *35*). An Odyssey data system (Finnigan FTMS, Madison, Wisconsin) acquired time-domain ICR data, Fourier transformed it, and processed the discrete mass spectrum into a peak list. The peak list was further analyzed with home-written software to calculate the extent of deuterium in the protein or peptides (*18*).

Determination of Inhibition Constant (K_i). The *Yersinia* PTPase activity was assayed at 25 °C in a reaction mixture (0.2 mL) containing appropriate concentrations of *p*-nitrophenyl phosphate (*p*NPP) as substrate. The buffer used was pH 7.0, 50 mM 3,3-dimethylglutarate, 1 mM DTT. The ionic strength of the solution was adjusted with NaCl to $I = 0.15$ M. The reaction was initiated by the addition of enzyme and quenched after 2−3 min by addition of 1 mL of 1 N NaOH. The nonenzymatic hydrolysis of the substrate was corrected by measurement of the optical density of the control without the addition of enzyme. The amount of product *p*-nitrophenol was determined from the absorbance at 405 nm, based on a molar extinction coefficient of 18 000 M^{-1} cm^{-1} (*30*). The inhibition constant for vanadate was determined for the *Yersinia* PTPase in the following manner. The initial rate at eight different *p*NPP concentrations ($0.2K_m$−$5K_m$) was measured at three different fixed inhibitor concentrations. The inhibition constant was obtained and the inhibition pattern was evaluated by use of a direct curve-fitting program KINETASYST (IntelliKinetics, State College, PA).

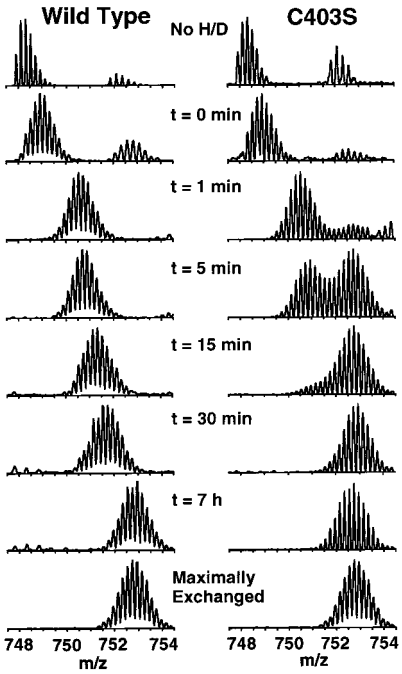

FIGURE 1: ESI−FT-ICR mass spectra of *Yersinia* PTPase segment, T202-C234 $[M + 5H]^{5+}$ ions, following various periods of solution-phase H/D exchange deuteration: left, wild-type PTPase; right, C403S mutant PTPase.

Isothermal Titration Calorimetry. All isothermal titration calorimetry experiments were performed with an OMEGA instrument from Microcal Inc., Northampton, MA. The experiments were conducted at 25 °C, in 50 mM 3,3-dimethylglutarate buffer, pH 7.0, containing 1 mM DTT. The ionic strength of the buffer was adjusted to 0.15 M by the addition of NaCl. Dilution for the protein during titration was determined by titration of the buffer into the protein solution. The heat of protein dilution was found to be negligible. The heat of ligand dilution was corrected by subtraction of the average heat of injection after saturation. The binding data were analyzed by use of Origin software (*36*). The binding constant, K, and the enthalpy change, ΔH, were used to calculate the free-energy change, ΔG, and the entropy change, ΔS, according to the following:

$$-RT \ln K = \Delta G = \Delta H - T\Delta S \quad (1)$$

RESULTS

Determination of Deuterium Content. Yersinia PTPase was diluted by addition of deuterated buffer (95% v/v), then incubated for various lengths of time; H/D exchange was quenched by lowering the pH to 2.2, and the deuterated sample was then subjected to either LC/MS analysis of the holoprotein or pepsin digestion followed by reverse-phase microbore LC/MS analysis of the proteolytic fragment peptides. Figure 1 shows ESI FT-ICR mass spectra of a proteolytic peptide, T202-C234, from both wild-type and C403S PTPase, after each of several different H/D exchange periods. Because online desalting (of intact PTPase) and

subsequent HPLC separation of its pepsin-cleaved segments are performed in H_2O, all fast-exchangeable hydrogens on the termini and side chains of the protein or peptides will back-exchange from deuterium to hydrogen, leaving deuteriums only for the peptide backbone amides.

It is important to understand that, because of the LC step, it is not possible experimentally to observe protein that is either 0% deuterated (because some backbone amide hydrogens will be replaced by deuteriums during quenching and digestion in ~50 atom % excess D_2O) or 100% deuterated (because the original buffer is 95% deuterated, and some deuteriums are lost during quench and digestion in ~50 atom % excess H_2O, HPLC separation in H_2O, and electrospray ionization). The course of deuteration must thus be scaled with respect to *minimally* deuterated (henceforth designated 0%, for an experiment in which protein is introduced directly into a 1:1 (v/v) mixture of quench buffer (100% H_2O) and 99.9% deuterated buffer, without prior 1:20 dilution into D_2O) and *maximally* deuterated (henceforth designated 100%) reference values.

The uppermost spectra in Figure 1 are for wild-type PTPase (left) and C403S PTPase (right) incubated and digested in H_2O (i.e., no H/D exchange). Although those spectra represent completely undeuterated protein, they do not provide a suitable reference point for monitoring deuteration. We therefore take the second spectrum from the top and the lowermost spectrum as minimally deuterated (i.e., protein diluted into 50% D_2O buffer and 50% quench buffer) and fully deuterated (i.e., 4 h of protein incubation in 95% D_2O buffer (pH meter reading = 6.1) and another 4 h after lowering the pH meter reading to 2.0), to serve as 0% and 100% references, respectively.

The deuterium content, D, for each partially deuterated protein (or segment) may be calculated from the following (*15*):

$$D = \frac{m - m_{0\%}}{m_{100\%} - m_{0\%}} H \qquad (2)$$

in which H is the total number of backbone amide hydrogens in the protein (or its segment), for example, $H = 292$ for *Yersinia* PTPase (after taking into account that the N-terminal residue and prolines have no exchangeable amide hydrogens). In eq 2, $m_{0\%}$, m, and $m_{100\%}$ are the average (i.e., the centroid of the isotope envelope) molecular weights for the minimally deuterated, partially deuterated, and maximally deuterated protein. All deuterium contents reported in this paper were calculated from eq 2. The back exchange for the intact protein and its proteolytic peptides were determined from the difference between the theoretical mass for maximally (95% D_2O) amide-deuterated species and the experimental mass determined after LC/MS analysis. For the intact protein, the extent of back exchange was ~37% (vs 18%−54% for various proteolytic peptides) during quench and LC/MS analysis. Those values are consistent with the 40%−50% of overall back exchange reported by other authors (*16*, *37*) and more recent 25%−55% values (*38*).

To assess the reproducibility of the above procedure, we performed three independent H/D exchanges on wild-type PTPase. After 1:20 dilution in deuterated buffer, each sample was incubated for 30 min at 25 °C, followed by LC-ESI FT-ICR analysis. Figure 2 shows the reproducibility

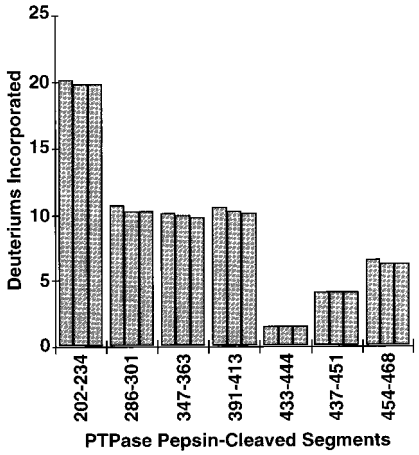

FIGURE 2: Deuterium incorporation following 1:20 dilution in deuterated buffer, 30 min of incubation of wild-type PTPase at 25 °C, quench and pepsin cleavage, and LC-ESI FT-ICR mass analysis. Note the excellent reproducibility (~0.5 Da or ~0.25 D atoms) for three independent H/D exchange experiments.

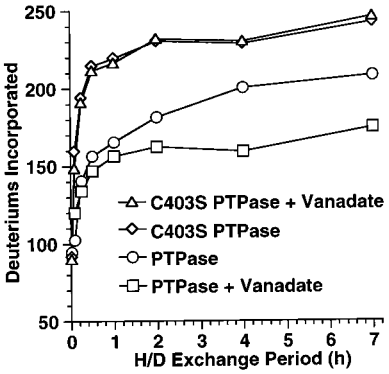

FIGURE 3: H/D exchange time courses for intact wild-type PTPase (○), wild-type PTPase plus vanadate (□), C403S PTPase (◇), and C403S PTPase plus vanadate (△). The catalytic domain was ~33 kDa.

in determined deuterium incorporation for several peptides obtained by pepsin digestion of the partially deuterated protein. The incorporated deuteriums are reproducible to within ~0.5 Da (i.e., ~0.25 D atoms).

Deuterium Incorporation for Intact PTPase. Figure 3 shows the H/D exchange behavior for intact wild-type and C403S mutant PTPases in the presence or absence of 220 μM vanadate at 25 °C. Up to ~208 (of a possible 292) backbone amine hydrogens can exchange with deuterium in the intact wild-type PTPase, within the first 7 h of H/D exchange. As a phosphate analogue, vanadate is a reversible and competitive inhibitor of PTPases (*31*, *39*). The crystal structure of the *Yersinia* PTPase/vanadate complex reveals that vanadate binds at the active site (*40*). At pH 7.0 and 25 °C, vanadate exhibits a reversible and competitive inhibition constant (K_i) of 1.0 ± 0.1 μM with the wild-type *Yersinia* PTPase (data not shown). Binding of vanadate inhibitor reduces substantially (by ~33) the number of deuteriums incorporated into the wild-type PTPase. In contrast, an additional ~35 backbone amide hydrogens exchange for deuterium in the C403S PTPase compared to wild-type PTPase. Interestingly, the extent of deuterium incorporation was essentially the same for the C403S mutant in the absence or presence of 220 μM vanadate. These striking observations dramatically illustrate that major changes

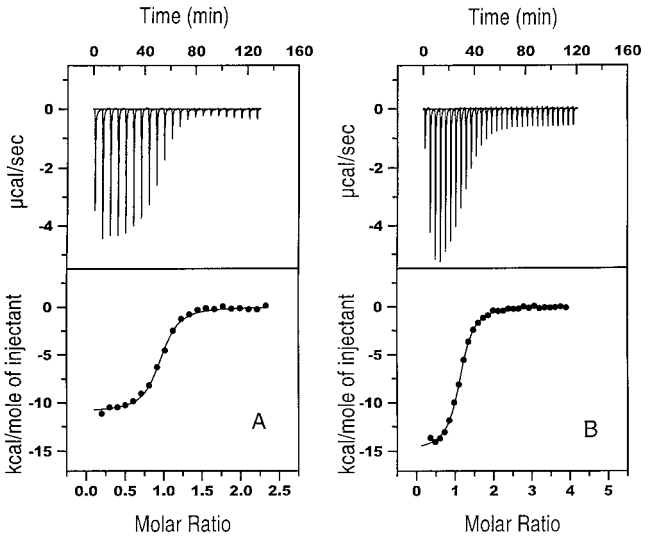

FIGURE 4: Calorimetric isothermal titration measurements of binding of vanadate to *Yersinia* PTPase (left) and the C403S mutant (right) at 25 °C and pH 7.0. Top Left: incremental heat effect upon titration of wild-type *Yersinia* PTPase (95 μM) by twenty 8-μL injections of vanadate (1.5 mM stock) at 6-min intervals. Top Right: incremental heat effect upon titration of the C403S *Yersinia* PTPase (74 μM) by thirty 8-μL injections of vanadate (1.5 mM stock) at 4-min intervals. Bottom: integrated curves showing experimental points obtained by integration of the upper peaks, as a function of the molar ratio of the vanadate to the *Yersinia* PTPase in the reaction cell. Each solid line corresponds to the best fit to the data by a nonlinear least-squares regression algorithm ORIGIN (*36*).

in the extent of H/D exchange can result from inhibitor binding or single-residue mutation, as discussed below.

Affinity of Vanadate for the C403S Mutant PTPase. Since vanadate does not affect the H/D exchange profile of the C403S mutant, we wondered whether C403S can still bind vanadate. Although the C403S mutant is catalytically inactive (*11*), it can still bind pTyr-containing peptides (*41*). Furthermore, the three-dimensional structure of the C403S mutant PTPase crystal grown with sulfate shows that this inhibitor occupies the active site (*42*). However, the true affinity of vanadate for the C403S mutant is unknown. Since the C403S mutant has no phosphatase activity, the K_i value for vanadate cannot be obtained from steady-state kinetic techniques. We therefore performed isothermal titration calorimetry experiments to determine the affinity of vanadate for the C403S mutant as well as the native *Yersinia* PTPase. The titration curves and binding isotherms are shown in Figure 4. The stoichiometry, *N*, for binding of vanadate is 1 for both proteins and the K_d (dissociation constant) is 1.3 $\pm$ 0.1 and 2.3 $\pm$ 0.1 μM for the wild type and the C403S mutant, respectively. Thus, the affinities of vanadate for the wild-type *Yersinia* PTPase determined by inhibition kinetics and titration calorimetry agree very well, and the affinity of vanadate for the C403S mutant is similar to that of the wild-type enzyme. Table 1 summarizes the thermodynamic parameters derived from the titration calorimetry experiments.

Mass Spectrometric Identification of Proteolytic Segments of PTPase. To localize the regions of *Yersinia* PTPase where hydrogen exchange was inhibited or increased by ligand binding or active site mutation, we performed H/D exchange experiments on the intact protein followed by pepsin digestion. Pepsin cleaves proteins somewhat nonspecifically to yield many peptide fragments, each of which could then be identified by ESI FT-ICR MS. The proteolytic segments were assigned by one or more of the following methods: (a) accurate mass measurements based on melittin as an internal calibrant (<10 ppm mass accuracy); (b) MS/MS spectra of peptides generated by the use of IRMPD (*32*); and (c) measured monoisotopic molecular weights based on external calibration (<25 ppm mass accuracy). An example of accurate mass measurement is shown in Table 2, for a particular proteolytic fragment peptide. Search of the *Yersinia* PTPase amino acid sequence yielded seven candidate peptides (residues 163−197, 323−356, 332−365, 349−382, 354−386, 397−430, and 398−431), each of whose monoisotopic molecular mass agrees with the experimental value to within 1 Da. However, the monoisotopc mass of only one of those peptides (residues 163−197) falls within 10 ppm of the experimental value. Remarkably, 67% of peptic peptides derived from PTPase could be identified in this way. Note that neither quadrupole nor time-of-flight mass analyzers have sufficient mass accuracy to achieve such results. For those segments for which two or more peptides matched the experimental monoisotopic molecular mass to within <5 ppm, infrared multiphoton dissociation (IRMPD) of the parent ions generated additional fragments, from which additional assignments could be made; another 18% of peptic peptides were identified in that way. Finally, a few low-concentration peptic peptides were identified from their measured monoisotopic molecular weights on the basis of external calibration and the known cleavage sites of *Yersinia* PTPase inferred from the results of the first two methods; another 15% of the peptic peptides were identified by that method. In all, some 33 segments, spanning 93.5% of PTPase primary amino acid sequence, were identified as shown in Figure 5.

Table 1: Thermodynamic Parameters Derived from the Titration of *Yersinia* PTPase with Vanadate at pH 7.0 and 25 °C

Yersinia PTPase	*N*	K_d (μM)	ΔH (kcal mol^{-1})	$T\Delta S$ (kcal mol^{-1})	ΔG (kcal mol^{-1})
wild-type	0.97 $\pm$ 0.01	1.3 $\pm$ 0.1	−10.0 $\pm$ 0.2	−2.0	−8.0
C403S	1.11 $\pm$ 0.01	2.3 $\pm$ 0.1	−14.9 $\pm$ 0.1	−7.2	−7.7

Table 2. Illustration of Peptide Identification from FT-ICR Accurate Mass Measurement[a]

peptide segment	monoisotopic mass	deviation from experimental value (ppm)
[P] M163-L197[S]	3682.78	2
[G] L323-D356[Q]	3682.85	21
[M] Y332-T365[K]	3681.90	236
[V] V349-M382[Y]	3681.84	252
[N] W354−K386[G]	3682.81	12
[K] L397-E430[D]	3681.84	252
[L] R398-D431[M]	3683.79	276

[a]The experimental peptide monoisotopic mass (i.e., all carbons are ^{12}C, all nitrogens are ^{14}N, all oxygens are ^{18}O, all hydrogens are ^{1}H, and all sulfurs are ^{32}S) is 921.70 for $(M + 4H)^{+}$, or $M = (921.70 \times 4) - (4 \times 1.007825) = 3682.77$ Da. The Table lists the all of the possible *Yersinia* PTPase fragment monoisotopic masses within 1 Da of the experimental value. Only one, [P] M163-L197[S], falls within 10 ppm and identifies the correct fragment. The brackets denote the amino acid preceding the amino terminus (or following the carboxy terminus) of the segment before proteolysis.

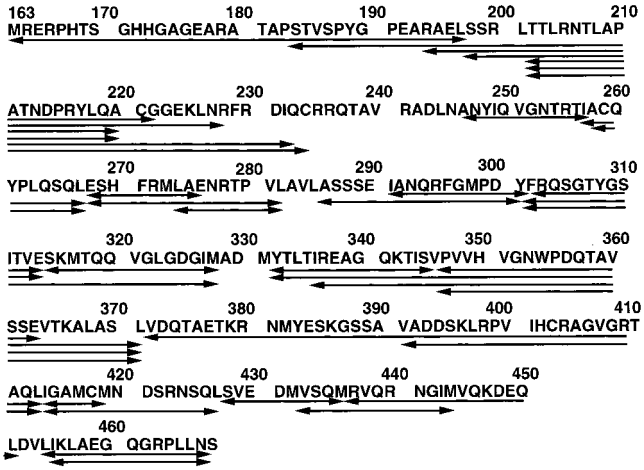

FIGURE 5: Amino acid sequence of wild-type PTPase, showing the pepsin-cleaved mass-identified fragments for which deuterium incorporation was measured.

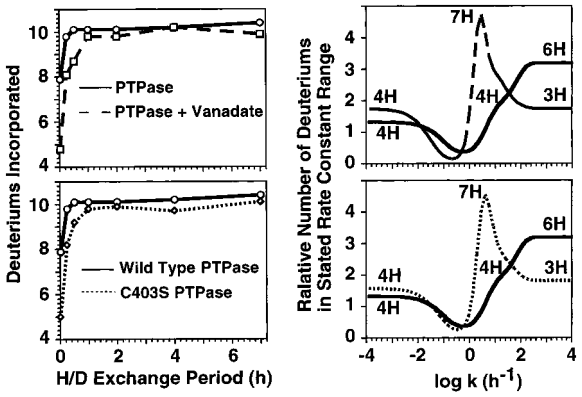

FIGURE 6: H/D exchange time courses (left) of segment P347-E363 (14 backbone amide protons) from wild-type PTPase (○), wild-type PTPase plus vanadate (□), and C403S PTPase (◇), analyzed by MEM to yield their H/D exchange rate constant distributions (right) for wild-type PTPase (—), wild-type PTPase plus vanadate (− − −), and C403S PTPase (•••). The number of backbone amide hydrogens for each resolved peak in the MEM-derived rate constant distribution is shown above that peak.

Time Course for Deuterium Incorporation for Various Proteolytic Segments. The next step in data analysis is to narrow the focus from the molecule as a whole to each of the proteolytic segments, by plotting the time course for deuterium incorporation for each of the 33 available proteolytic peptide segments. For ligand-free and complexed wild-type PTPase and C403S mutant PTPase, many peptic peptides exhibited essentially identical extents of deuterium incorporation. That is actually good, because it means that only part of the PTPase structure affects solvent accessibility by mutation and/or inhibitor binding. Fortunately, seven segments showed significant differences in the extent of deuterium incorporation in the complexed wild-type PTPase or C403S PTPase compared to uncomplexed wild-type PTPase (Figure 6, left; Figure 7). For example, compared to wild-type unliganded PTPase, the extent of deuterium incorporation decreases significantly in proteolytic segments constituting residues 202−234, 286−301, 347−363, 391−413, 433−444, and 437−451 on binding of vanadate, whereas a single-site mutation (C403S) results in decreased (compared to wild-type unliganded PTPase) deuterium incorporation for residues 347−363 but increased incorporation for residues 202−234, 391−413, 433−444, 437−451,

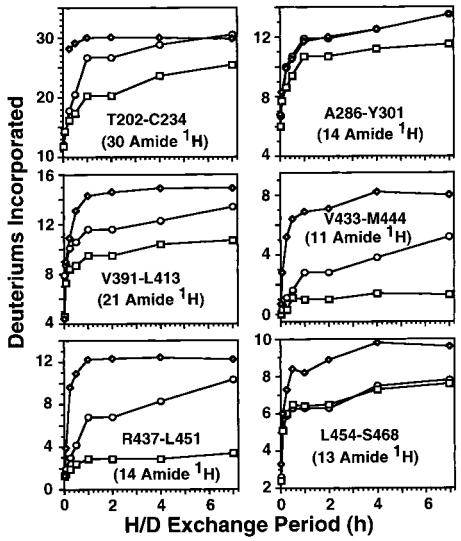

FIGURE 7: H/D exchange time courses for each of six different segments from wild-type PTPase (○), wild-type PTPase plus vanadate (□), and C403S PTPase (◇). The number of potentially exchangeable backbone amide hydrogens in each segment is shown in each panel.

and 454−468. The extents of deuterium incorporation within all proteolytic segments in the complexed and uncomplexed C403S PTPase (in the presence or absence of 220 μM vanadate) are essentially the same (data not shown).

Amide Hydrogen Exchange Rate Constant Distribution for Seven Selected Segments. One would like to focus even more narrowly, ultimately down to the single-residue resolution of high-resolution ^{1}H,^{15}N-heteronuclear single quantum correlation spectroscopy (HSQC) NMR (*18*). Although that is not generally possible by mass analysis (unless one is lucky enough to generate a pair of fragment peptides with a common terminus but differing by a single amino acid at the other end (*18*)), we can at least map the distribution in H/D exchange rate constants by subjecting the experimental deuterium uptake time course data to maximum entropy method (MEM) analysis (18). Figure 6 (right) and Figure 8 show MEM-derived H/D exchange rate constant distributions for each of 7 peptides, based on the time-course data of Figure 6 (left) and Figure 7. For reference, the total number of potentially exchangeable amide hydrogens for each segment is shown in each panel. For example (Figure 7, top left), one might expect 234 − 202 = 32 possible exchangeable amide hydrogens for the T202-C234 segment, but Figure 5 shows that there are two prolines (each with no exchangeable amide hydrogen) in that segment, so that only 30 amide hydrogens are potentially exchangeable.

Interpretation of the MEM plots requires a little explanation. For well-resolved peaks, the ordinate in Figure 6 (right) and Figure 8 is scaled so that the total area under each peak corresponds to the total number of amide hydrogens for that segment, over the corresponding range of exchange rate constants (the abscissa is actually the log of the rate constant) (*18*). The number of exchangeable backbone amide hydrogens calculated from the area under each resolved peak appears at the top of that peak. However, if the rate constant is too slow (or too fast) to be determined from the experimental data, the MEM plot simply levels off to a horizontal line extending infinitely to the left (or right); in Figure 6 (right), for example, one cannot distinguish between

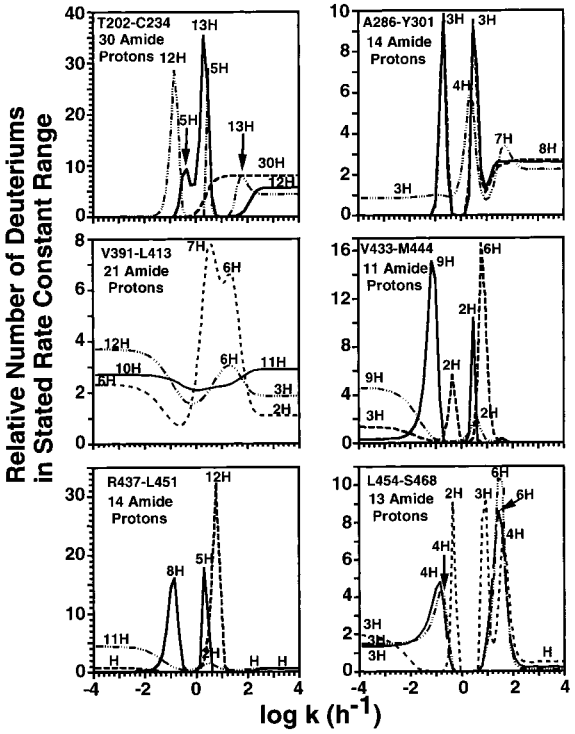

FIGURE 8: H/D exchange rate constant distributions derived from the H/D exchange time courses for each of the six different segments shown in Figure 6: wild-type PTPase (—), wild-type PTPase plus vanadate (– – –), and C403S PTPase (•••). The total number of backbone amide hydrogens for each segment appears just below the segment initial and final amino acid residues. The number of backbone amide hydrogens for each resolved peak in the MEM-derived rate constant distribution is shown above that peak.

rate constants slower (or faster) than limiting values of $\sim 10^{-2}$ or $\sim 10^{2}$ h^{-1}.

Back exchange for the intact *Yersinia* PTPase protein (37%) differs from that for its peptic fragment peptides (18%−54%) in our experiments. In our use of MEM to convert raw time-course data to a distribution in H/D exchange rate constants, we specify only the (known) total number of exchangeable amide hydrogens and the measurement error for the deuteriums incorporated.

Although it is possible to infer conformational and/or dynamic changes within individual segments of PTPase from the difference in exchange rate constant distribution induced by ligand binding and/or active site mutation (Figure 6, right; Figure 8), we find it easiest to consider the results graphically, by color-coding segments of a three-dimensional X-ray single-crystal diffraction ribbon structure (Figure 9) according to whether the ligand binding or mutation increases (red) or decreases (blue) the H/D exchange rate constants for that segment. In Figure 9 (top), we represent H/D exchange rate changes induced by C403S mutation by color-coding of the X-ray structure for the sulfate-bound C403S mutant PTPase (*42*). Because the coordinates for the vanadate-bound *Yersinia* PTPase are not available, we represent H/D exchange rate changes induced by vanadate binding by color-coding the X-ray structure of the tungstate-bound wild-type PTPase (*9*), as shown in Figure 9 (bottom).

Two Exchange Rates for the T202-C234 Segment in the C403S PTPase. One special case deserves mention. For the T202-C234 segment of C403S PTPase, Figure 1 (right)

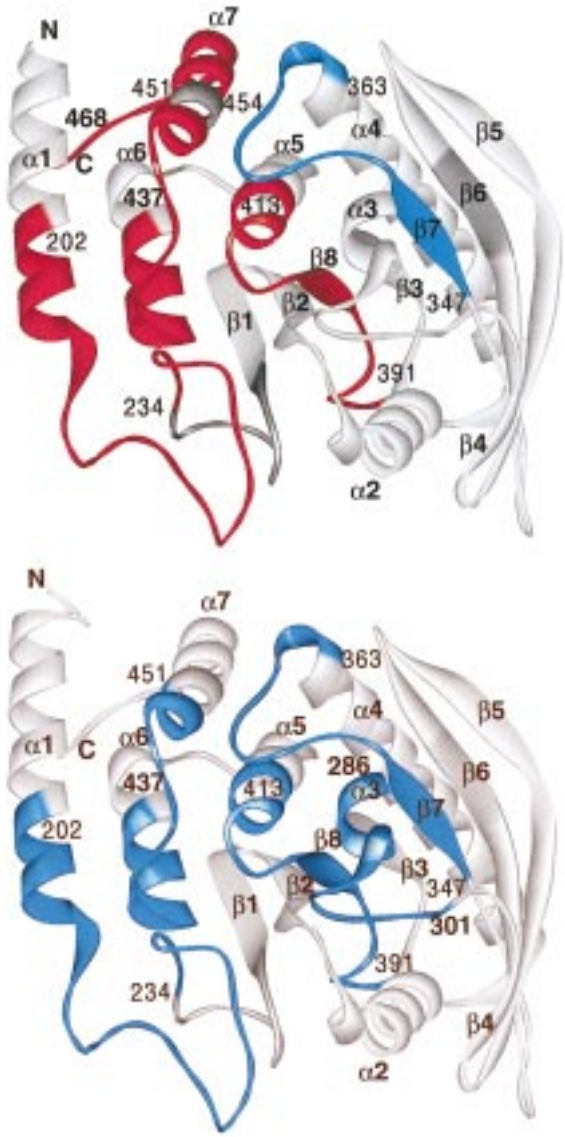

FIGURE 9: Ribbon diagrams of the three-dimensional single-crystal X-ray diffraction structures of the complex of C403S mutant PTPase with sulfate (top) and the complex of wild-type PTPase with tungstate (bottom) (*9*), drawn with WebLab Viewer. The (relatively few) unobserved segments are shaded in dark gray. Color coding represents faster (red), slower (blue), or unchanged (grey) deuterium exchange relative to wild-type PTPase, for C403S mutant PTPase (top) and vanadate-inhibited PTPase (bottom).

clearly shows two different rates of amide hydrogen exchange, whereas Figure 1 (left) reveals a single H/D exchange rate for wild-type PTPase. For C403S PTPase mutant, a slow-exchange component appears initially (up to ~10 min), after which exchange proceeds faster than for the wild-type PTPase.

DISCUSSION

Visualization of Effects of Mutation and Vanadate Binding on PTPase Solvent Accessibility. In attempting to visualize the H/D exchange results, we face the immediate problem that X-ray structures are not available for either the ligand-free C403S mutant or the vanadate-bound wild-type PTPase. Since the C403S PTPase exists in the WpD loop closed conformation, we represent changes in H/D exchange for C403S PTPase versus wild-type PTPase by color-coding

segments of the known structure of C403S/sulfate complex (Figure 9, top), and changes in H/D exchange for vanadate-inhibited PTPase versus wild-type PTPase by color-coding segments of the known structure of tungstate-bound wild-type PTPase (Figure 9, bottom). Thus, the color-coded results in Figure 9 (top) show that, except for reduced solvent accessibility for the WpD loop itself, the conformation of the C403S PTPase is much more open and/or more flexible than that of native PTPase. Compared to the unliganded wild-type PTPase, the vanadate-bound wild-type PTPase (Figure 9, bottom) displays reduced solvent accessibility for both the WpD loop and surrounding loops in the active site.

WpD Loop. A catalytic general acid Asp 356 and an invariant tryphophan (Try 354) are found in the WpD loop (residues 350−360). X-ray crystal structures show that the WpD loop closes by moving toward the phosphate-binding loop by up to 6 Å on binding of tungstate inhibitor to wild-type PTPase (*8*, *9*, *42*). The WpD loop is also in the closed conformation in the crystal structure of C403S mutant in its complex with sulfate (*42*). Crystallographic studies reveal no noticeable differences between the ligand-bound structures of the wild-type *Yersinia* PTPase and the C403S mutant. Spectroscopic studies (*10*) indicate that in solution the unliganded wild-type *Yersinia* PTPase exists as an equilibrium mixture of almost equal populations of WpD loop closed and open conformations. As expected, the WpD loop exists predominantly in the closed conformation in the arsenate-complexed wild-type *Yersinia* PTPase. Surprisingly, the ligand-free and ligated C403S mutant *Yersinia* PTPase's remain mostly in the WpD loop closed conformation in solution. Thus, the C403S mutant WpD loop conformation is independent of the presence of a ligand (*10*). Consistent with previous spectroscopic data, Figure 6 (left) shows that fewer deuteriums are incorporated, after 30 min of H/D exchange, into the P347-E363 segment (which includes the WpD loop) of the vanadate-bound wild-type PTPase or the C403S mutant than in the ligand-free wild-type PTPase, presumably because the WpD loop has closed over the active site to limit solvent access. More specifically, Figure 6 (right) shows that three P347-E363 segment amide hydrogens with fast exchange rates ($k \geq 100\ h^{-1}$) in the wild-type PTPase slow to $\sim 3\ h^{-1}$ in both vanadate-inhibited wild-type PTPase and C403S mutant.

Hydrogen exchange of a protein segment which alternates between open and closed conformations can be described by the following simple two-state model (*43*):

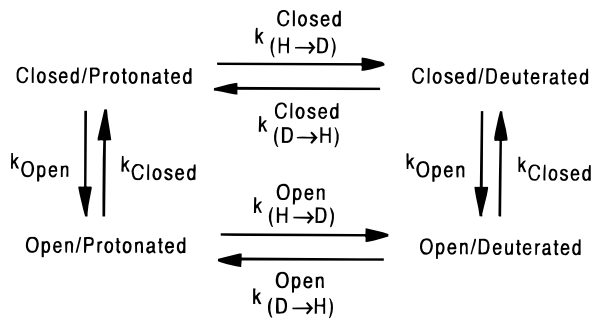

This model simply implies that hydrogen exchange may occur (with different rates) in both closed and open forms of the loop and that the loop closing/opening rates are not affected by replacement of amide hydrogens by deuteriums. There are two possible rate-limiting steps in the exchange of amide hydrogens: (1) loop opening, the so-called EX1 mechanism, or (2) the exchange reaction, the EX2 mechanism (*14*, *44*, *45*). The hydrogen exchange rate is required to be faster than the closing rate for the EX1 mechanism. In this case the measured exchange rate yields k_{open} directly. Conversely, the EX2 mechanism requires that the exchange rate be slower than the closing rate. Experimentally, we observe only a single (fast) exchange rate for the WpD loop in the uncomplexed wild-type PTPase, presumably because the interconversion between the loop open and closed states is fast compared to the H/D exchange rate. The ligand-free wild-type enzyme alternates between open- and a closed-loop forms with a rate constant of $\sim 2.6 \times 10^8\ s^{-1}$ ($= 9.4 \times 10^{11}\ h^{-1}$) based on time-resolved fluorescence anisotropy (*10*).

Conformational or Dynamic Changes of Yersinia PTPase Effected by Ligand Binding. The number of deuteriums incorporated into intact wild-type PTPase in the presence of 220 μM vanadate ($K_I \approx 1\ \mu M$) decreases by 33 compared to PTPase alone (Figure 3). Vanadate is a small tetrahedral oxyanion and cannot directly influence 33 deuteriums. The only explanation for such a large overall decrease in H/D exchange is that binding of vanadate leads to a conformational change that reduces solvent accessibility for 33 backbone amide hydrogens.

Vanadate is thought to act as a transition-state analogue for the PTPase-catalyzed reaction due to its tendency to adopt a pentavalent geometry. Based on the continuous electron density between the bound vanadate and the active site Cys403 in the *Yersinia* PTPase, it was concluded that a covalent bond is formed between the Sγ atom of Cys403 and the vanadium atom so that the vanadate ion forms a pentavalent trigonal bypyramidal structure that resembles the transition state (*40*). In solution, vanadate inhibits the *Yersinia* PTPase-catalyzed reaction reversibly and competitively, with a dissociation constant of 1 μM. Thus, at 220 μM vanadate, virtually all PTPase molecules are complexed to vanadate. Interestingly, the mass determined by ESI−FT-ICR MS for electrosprayed vanadate-bound PTPase was the same as that for PTPase alone. Therefore, either the binding is not covalent, or the S−V bond is unstable and is broken during electrospray ionization.

Solvent accessibility decreases in several loops/turns in the vanadate-complexed PTPase relative to ligand-free wild-type PTPase. Vanadate binding decreases deuterium incorporation (Figure 7, □) and slows the exchange rates of many amide hydrogens (Figure 8, − − −) in each of the PTPase segments comprising residues 202−234, 286−301, 391−413, 433−444, and 437−451. These results may be understood by comparing the three-dimensional crystal structures of PTPase with and without tungstate in the active site (ribbon diagrams in Figure 9 (bottom) (*8*)). Segments may be classified as follows. Residues 202−234 constitute helix α1 and turn $\alpha 1-\beta 1$; residues 286−301 constitute helix α3 (a short α-helix) and turn $\alpha 3-\beta 4$; residues 391−413 constitute turn $\alpha 4-\beta 8$, sheet β8 (a short β-sheet), turn $\beta 8-\alpha 5$, and helix α5; and residues 433−451 constitute helix α6 and turn $\alpha 6-\alpha 7$. The catalytic site centers around the phosphate-binding loop formed between β8 and α5 (residues 403−410) and is surrounded by the residues contributed by the turns, including $\alpha 1-\beta 1$, helix α3, $\alpha 3-\beta 4$, and $\alpha 6-\beta 7$

(*8*). Comparison of the ligand-free and bound structures clearly shows that binding of tungstate pulls the WpD loop down to cover much of the active site. It is therefore not surprising to find that solvent accessibility for the vanadate-inhibited PTPase (Figure 9 (bottom)) is substantially reduced, not only for the WpD loop itself but also throughout several neighboring segments known to form the active site that are evidently shielded by the closed WpD loop. Although the vanadate-induced closing of the WpD loop is visually obvious by comparison of the ribbon diagrams for wild-type and tungstate-inhibited PTPase (*8*, *42*), those X-ray structures are otherwise very similar for the various blue-coded loops for which a major decrease in solvent accessibility is observed on binding of vanadate. Vanadate binding must therefore act not only to close the WpD loop but also to tighten up much of the remaining structure so as to reduce solvent access.

The phosphate-binding loop formed between β8 and α5 (residues 403−410) positions the bound oxyanion directly over Cys403 by anchoring three of the anion's oxygens to the inward pointing main-chain amides of residues 404−409 through hydrogen bonds (*8*). This unique structure of the phosphate-binding loop is maintained by a series of hydrogen-bonding interactions involving the backbone carbonyl groups of the loop and side chains radiating out from the loop. These include the following conserved and mostly buried residues: His402, Asn245 (located in α1−β1), Tyr301 (located in α3−β4), and Arg437 and Arg440 (located in α6−α7) (*8*). In addition, the oxyanion in the active site preferentially stabilizes the WpD loop closed conformation by forming a bidentate hydrogen bond with the guanidinium group of Arg409 (*46*), whose position is fixed by a coplanar salt bridge between the guanidinium group and the carboxylate of Glu290 (located in α3) (*42*). These changes in the active site lead to the formation of a new hydrogen bond between the Nη1 of Arg409 and the carbonyl oxygen of Trp354 (in the WpD loop) and optimize the van der Waals between the aliphatic portion of the Arg409 side chain and the indole side chain of Trp354 (*42*). These interactions are essential for the WpD loop to stay in the closed conformation in the presence of the oxyanion and allow additional hydrogen bonds between the apical oxygen of the oxyanion and Asp356, Gln357, Gln446, and Gln450 (α6−α7) (*9*). Finally, residues Phe229 and Ile232 form part of the binding pocket for the tyrosine ring of the substrate (*9*, *47*).

Consistent with the X-ray structural information, our H/D exchange data show that the presence of vanadate in the active site of *Yersinia* PTPase protects hydrogens derived from residues that are in direct contact with the oxyanion and residues that stabilize the active site structure. Since, with the exception of the WpD loop, the structures of the ligand-free and ligand-bound *Yersinia* PTPase are superimposable, the observed decrease in H/D exchange rate in the regions noted above implies reduced dynamics in the active site due to vanadate binding. Because vanadate is a transition-state analogue, these binding interactions stabilize and optimize the orientation of active site residues involved in substrate binding and catalysis. Thus, H/D exchange followed by FT-ICR MS provides an extraordinarily sensitive probe of protein conformational/dynamic changes followed by ligand binding. PTPase catalysis involves a conformational change restricted to the movement of the WpD loop that can be described as a hinged loop movement. Since only the ligand-bound structures have been solved for the dual specificity phosphatases and the low molecular weight phosphatases, it remains to be established whether similar loop movement also occurs in these two families of enzymes. This question can be answered by the techniques described in this work.

Conformational or Dynamic Changes of Yersinia PTPase Affected by Active Site Mutation. The nucleophilic thiol group of Cys403 in the active site of *Yersinia* PTPase attacks the phophorus atom in a substrate. Although sulfhydryls in proteins typically exhibit acid dissociation pK_a's of ∼8.5, the side chain of Cys403 has an apparent pK_a of ∼4.7 (*48*). At physiological pH, the thiolate anion is stabilized by hydrogen bonds between the backbone amides of the phosphate-binding loop, helix α5 (*8*, *49*, *50*), and the side chains of His402 and Thr410 (*48*, *51*). Thus, the Cys403 to Ser mutation is not a simple substitution of OH for SH, but rather a replacement of the negatively charged thiolate with a neutral hydroxyl group. Structural and/or dynamic features that are important for the stabilization of the thiolate in the wild-type PTPase may have to be readjusted in order to accommodate the neutral hydroxyl group. To date, no X-ray crystal structure of ligand-free C403S mutant PTPase is available. Spectroscopic and functional studies show that although the overall secondary and tertiary structural elements are similar for wild-type and C403S PTPase, there are noticeable conformational differences in their active sites, and the structure of C403S PTPase is significantly less stable than that of wild-type PTPase: that is, the free energy of unfolding for the wild-type PTPase is 6.14 kcal/mol versus 4.02 kcal/mol for the mutant (*11*). In addition, the WpD loop in the C403S mutant adopts the closed conformation irrespective of whether arsenate is present (*10*). The loss of the negative charge in the active site may lead to subtle alterations in the structure of the active site and/or perturb the electrostatic balance between the phosphate-binding loop and the WpD loop, both of which may contribute to the collapse of the WpD in the C403S mutant. It is therefore not surprising that a single S to O atom substitution in the nucleophile (namely, Cys to Ser mutation) renders PTPase catalytically inactive (*2*, *11*).

Compared to the wild-type PTPase, the unliganded C403S mutant displays a decreased deuterium incorporation into the WpD loop (residues 347−363) indicating a closed WpD loop conformation, consistent with UV resonance Raman data (*10*). Interestingly, active site mutation (C403S) results in ∼35 more exchanged deuteriums into the C403S mutant compared to the wild-type PTPase, suggesting a more open conformation and/or faster exchange in the mutant protein. Our H/D exchange results clearly show that the extent of deuteriums incorporated increases (Figure 7, ◇) and the exchange rates of some amide hydrogens increase (Figure 8, - - -) in the unliganded C403S mutant relative to the wild-type PTPase, in each of the segments comprising residues 202−234 (α1 and turn α1−β1), 391−413 (turn α4−β8), 433−444 (α6), 437−451 (α6 and turn α6−α7), and 454−468 (α7). We suggest that the active site thiolate anion in the wild-type enzyme may be responsible for holding the phosphate-binding loop and the surrounding loops together. Loss of the negative charge in the C403S mutant results in more relaxed dynamics in the active site region. Unlike

residues 202−234, 391−413, and 433−444, which center or surround the catalytic site, residues 454−468 constitute the C-terminus of the protein. These data support the hypothesis that the conformational/dynamic properties of the active site as well as other parts of the C403S mutant differ from those in the native enzyme. Indeed, $^{1}H-^{15}N$ HSQC 2D NMR experiments reveal global differences in the main-chain amide chemical shifts between the C403S mutant and the wild-type *Yersinia* PTPase (Zhang, Y.-L. and Zhang, Z.-Y., unpublished data).

It is also interesting to note that there are two distinct exchange rates during the initial 15 min of H/D exchange for the peptide comprising residues 202−234 (α1 and turn α1−β1) in the C403S mutant (Figure 1, right). The mass distributions for these two exchange processes also vary as exchange proceeds. In contrast, only one (slow) exchange rate is observed for the native PTPase (Figure 1, left). We infer that helix α1 and turn α1−β1 are not stable in the C403S PTPase, and that there is an interconversion between the open and closed conformations. That interconversion is slow enough that two exchange rates are observed at the beginning of the exchange period. After ∼30 min, only one (fast) exchange rate dominates, and all 30 backbone amide hydrogens exchange within an hour. The rate constant, k_{open}, for this segment can be estimated as $\sim 15\ h^{-1}$ from the rate of increase in relative abundance of the high *m*/*z* envelope.

Dynamic and Thermodynamic Properties of Ligand Binding to the C403S Mutant Yersinia PTPase. In contrast to the wild-type *Yersinia* PTPase, the presence of 220 μM vanadate does not affect the H/D exchange behavior of the C403S mutant, that is, the WpD loop stays closed and deuterium incorporation is enhanced in the peptide segments noted above. Can the C403S mutant bind vanadate? It is known that the Cys to Ser mutant PTPase can still bind pTyr-containing substrates. A sulfate is located at the active site of the structure of C403S crystallized in the presence of 200 mM Li_2SO_4 (*42*). The structure of the C403S−sulfate complex is identical to that of the native PTPase complexed with tungstate. Presumably, vanadate in solution complexes with the C403S in a similar fashion. In addition, the C403S mutant also possesses similar affinity for the competitive inhibitor suramin compared to the wild-type enzyme (*52*).

The affinity of C403S for vanadate and the thermodynamic parameters associated with binding were measured with an isothermal titration calorimeter (Figure 4). The dissociation constant of C403S for vanadate is 2.3 μM, which is similar to that of the wild-type PTPase (1.3 μM, Table 1). Thus, although the conformational/dynamic properties of the C403S mutant differ significantly from those of the wild-type PTPase, they display nearly identical affinity (and free energy of binding, Δ*G*) for vanadate. As shown in Table 1, the Δ*H* and *T*Δ*S* for the binding of vanadate to the *Yersinia* PTPase are −10.0 and −2.0 kcal/mol, respectively, indicating that vanadate binding is an enthalpically favorable but entropically unfavorable reaction, that is, the binding of vanadate to *Yersinia* PTPase is driven primarily by enthalpy. That result is consistent with structural data that hydrogen bonding or ionic interactions between vanadate and the PTPase active site play a major role in binding. The slightly unfavorable *T*Δ*S* term for vanadate binding suggests that the enhanced enthalpic interaction comes with a price of a decrease in the entropy of the PTPase−vanadate complex, which more than offsets the favorable entropic gain due to the desolvation of the oxyanion.

The Δ*H* and *T*Δ*S* for the binding of vanadate to the C403S mutant are −14.9 and −7.2 kcal/mol, respectively, indicating that the binding of vanadate to C403S is also driven by enthalpy. Although the enthalpic contribution to the binding of vanadate for C403S is 4.9 kcal/mol more favorable than for the wild-type enzyme, the entropic contribution is disfavored by 5.2 kcal/mol. Evidently the interaction between C403S and vanadate involves enthalpy/entropy compensation, namely, perturbations that decrease the enthalpy can also decrease the entropy, with little or no effect on the free energy, so that changes in enthalpy are not independent of changes of entropy. The enhanced enthalpic term for the association of C403S with vanadate may be explained by the removal of the repulsive interaction between the thiolate and the negatively charged vanadate in the wild-type PTPase. Evidently, this increased electrostatic interaction also leads to a reduction of entropy in the vanadate-bound state. Although the molecular nature and origin for the reduced entropic term for binding are unclear, collectively, the thermodynamic data support the conclusion (reached from spectroscopic experiments and the H/D exchange experiments described above) that the conformation and/or dynamic properties of the C403S mutant are different from those of the native *Yersinia* PTPase. The results described herein highlight the need to characterize carefully site directed mutant enzymes before reaching any definitive mechanistic conclusions. In this case, although the structure of the ligand-bound C403S is similar to that of the wild-type enzyme, and C403S has similar affinity for vanadate as the wild-type PTPase, the conformational and dynamic properties of the two proteins still differ.

Advantages of FT-ICR MS for H/D Exchange Rate Measurement. FT-ICR offers several unique advantages over other forms of mass spectrometry for hydrogen exchange analysis. First, by virtue of its ultrahigh mass measurement accuracy, most of the proteolytic segments of a protein can be identified by their accurate mass alone, thereby reducing the need for MS/MS or other partial sequencing of each segment. Second, because of FT-ICR's ultrahigh mass resolution, isotopic peaks of all proteolytic segments are well-resolved, facilitating charge state assignment as well as distinguishing between close or overlapped isotopic distributions from different proteolytic segments. Third, multiple rates of uptake of deuterium by different conformers of a single proteolytic segment may be resolved: for example, two exchange rates for segment 202−234 in C403S PTPase (Figure 1, right). Finally, the number of incorporated deuteriums may be determined to within 0.5 Da (i.e., 0.25 deuteriums), or to within ∼3% in this work, compared to within ∼5% in prior reports (*15*, *37*). Note that 0.5 Da (0.25 incorporated deuteriums) represents the *reproducibility* of the LC-ESI FT-ICR MS measurements evaluated from three independent runs, including errors introduced from H/D exchange, quenching, pepsin digestion, HPLC, and FT-ICR MS. FT-ICR mass *accuracy* itself is typically within 25 ppm based on external calibration; for an ion of ∼3000 Da, the mass accuracy is within 0.08 Da. Thus, our precision for counting incorporated deuteriums is somewhat poorer than the accuracy of the mass measurement itself.

ACKNOWLEDGMENT

The authors thank M. A. Freitas for suggesting software to generate the 3D structures, S. D.-H. Shi for helpful discussion about internal mass calibration, and J. P. Quinn for instrumentation advice.

REFERENCES

1. Zhang, Z.-Y. (1998) *Crit. Rev. Biochem. Mol. Biol. 33*, 1−52.
2. Guan, K. L., and Dixon, J. E. (1991) *J. Biol. Chem. 266*, 17026−17030.
3. Cho, H., Krishnaraj, R., Bannwarth, W., Walsh, C. T., and Anderson, K. S. (1992) *J. Am. Chem. Soc. 114*, 7296−7298.
4. Zhang, Z.-Y., Wang, Y., and Dixon, J. E. (1994) *Proc. Natl. Acad. Sci. U.S.A. 91*, 1624−1627.
5. Guan, K. L., and Dixon, J. E. (1990) *Science 249*, 553−556.
6. Bolin, I., and Wolf-Watz, H. (1988) *Mol. Microbiol. 2*, 237−245.
7. Bliska, J. B., Guan, K. L., Dixon, J. E., and Falkow, S. (1991) *Proc. Natl. Acad. Sci. U.S.A. 88*, 1187−1191.
8. Stuckey, J. A., Schubert, H. L., Fauman, E. B., Zhang, Z.-Y., Dixon, J. E., and Saper, M. A. (1994) *Nature 370*, 571−575.
9. Fauman, E. B., Yuvaniyama, C., Schubert, H. L., Stuckey, J. A., and Saper, M. A. (1996) *J. Biol. Chem. 271*, 18780−18788.
10. Juszczak, L. J., Zhang, Z.-Y., Wu, L., Gottfried, D. S., and Eads, D. D. (1997) *Biochemistry 36*, 2227−2236.
11. Zhang, Z. Y., and Wu, L. (1997) *Biochmeistry 36*, 1362−1369.
12. Englander, S. W., and Kallenbach, N. R. (1984) *Q. Rev. Biophys. 16*, 521−655.
13. Gregory, R. B., and Rosenberg, A. (1986) in *Methods in Enzymology* (Hirs, C. H. W., and Timasheff, S. N., Eds.) pp 448−508, Academic Press, Orlando, FL.
14. Englander, S. W., and Mayne, L. (1992) *Annu. Rev. Biophys. Biomol. Struct. 21*, 243−265.
15. Zhang, Z., and Smith, D. L. (1993) *Protein Sci. 2*, 522−531.
16. Johnson, R. S., and Walsh, K. A. (1994) *Protein Sci. 3*, 2411−2418.
17. Wang, F., Blanchard, J. S., and Tang, X.-j. (1997) *Biochemistry 36*, 3755−3759.
18. Zhang, Z., Li, W., Logan, T. M., Li, M., and Marshall, A. G. (1997) *Protein Sci. 6*, 2203−2217.
19. Buchanan, M. V., and Hettich, R. L. (1993) *Anal. Chem. 65*, 245A−259A.
20. Amster, I. J. (1996) *J. Mass Spectrom. 31*, 1325−1337.
21. Dienes, T., Pastor, S. J., Schürch, S., Scott, J. R., Yao, J., Cui, S., and Wilkins, C. L. (1996) *Mass Spectrom. Rev. 15*, 163-211.
22. Laude, D. A., Stevenson, E., and Robinson, J. M. (1997) in *Electrospray Ionization Mass Spectrometry* (Cole, R. B., Ed.) pp 291−319, John Wiley and Sons, Inc., New York.
23. Green, M. K., and Lebrilla, C. B. (1997) *Mass Spectrom. Rev. 16*, 53−71.
24. Marshall, A. G., Hendrickson, C. L., and Jackson, G. S. (1998) *Mass Spectrom. Rev. 17*, 1−35.
25. McLafferty, F. W. (1994) *Acc. Chem. Res. 27*, 379−386.
26. Wu, Q., Van Orden, S., Cheng, X., Bakhtiar, R., and Smith, R. D. (1995) *Anal. Chem. 67*, 2498−2509.
27. Senko, M. W., Hendrickson, C. L., Pasa-Tolic, L., Marto, J. A., White, F. M., Guan, S., and Marshall, A. G. (1996) *Rapid Commun. Mass Spectrom. 10*, 1824−1828.
28. Kelleher, N. L., Senko, M. W., Siegel, M. M., and McLafferty, F. W. (1997) *J. Am. Soc. Mass Spectrom. 8*, 380−383.
29. Marshall, A. G., Senko, M. W., Li, W., Li, M., Dillon, S., Guan, S., and Logan, T. M. (1997) *J. Am. Chem. Soc. 119*, 433−434.
30. Zhang, Z.-Y., Clemens, J., Schubert, H., Stuckey, J., Fisher, M., Hume, D., Saper, M., and Dixon, J. (1992) *J. Biol. Chem. 267*, 23759−23766.
31. Wu, L., Buist, A., den Hertog, J., and Zhang, Z.-Y. (1997) *J. Biol. Chem. 272*, 6994−7002.
32. Little, D. P., Speir, J. P., Senko, M. W., O'Cornnor, P. B., and McLafferty, F. W. (1994) *Anal. Chem. 66*, 2809−2815.
33. Marshall, A. G., Wang, T.-C. L., and Ricca, T. L. (1985) *J. Am. Chem. Soc. 107*, 7893−7897.
34. Guan, S., and Marshall, A. G. (1996) *Int. J. Mass Spectrom. Ion Processes 157/158*, 5−37.
35. Senko, M. W., Hendrickson, C. L., Emmett, M. R., Shi, S. D.-H., and Marshall, A. G. (1997) *J. Am. Soc. Mass Spectrom. 8*, 970−976.
36. Wiseman, T., Williston, S., Brandts, J., and Lin, L.-N. (1989) *Anal. Biochem. 179*, 131−137.
37. Johnson, R. S. (1996) *J. Am. Soc. Mass Spectrom. 7*, 515−521.
38. Wang, F., Scapin, G., Blanchard, J. S., and Angeletti, R. H. (1998) *Protein Sci. 7*, 293−299.
39. Huyer, G., Liu, S., Kelly, J., Moffat, J., Payette, P., Kennedy, B., Tsaprailis, G., Gresser, M. J., and Ramachandran, C. (1997) *J. Biol. Chem. 272*, 843−851.
40. Denu, J. M., Lohse, D. L., Vijayalakshmi, J., Saper, M. A., and Dixon, J. E. (1996) *Proc. Natl. Acad. Sci. U.S.A. 93*, 2493−8.
41. Bliska, J. B., Clemens, J. C., Dixon, J. E., and Falkow, S. (1992) *J. Exp. Med. 176*, 1625−1630.
42. Schubert, H., Faumen, E., Stucky, J., Dixon, J., and Saper, M. (1995) *Protein Sci. 4*, 1904−1913.
43. Zhang, Z., Li, W., Li, M., Logan, T. M., Guan, S., and Marshall, A. G. (1997) *Techniques in Protein Chemistry VIII* (Marshak, D. R., Ed.) pp 703−713, Academic Press, San Diego, CA.
44. Creighton, T. E. (1990) *Biochem. J. 270*, 1.
45. Englander, S. W., and Poulsen, A. (1969) *Biopolymers 7*, 379−393.
46. Zhang, Z.-Y., Wang, Y., Wu, L., Fauman, E., Stuckey, J. A., Schubert, H. L., Saper, M. A., and Dixon, J. E. (1994) *Biochemistry 33*, 15266−15270.
47. Jia, Z., Barford, D., Flint, A. J., and Tonks, N. K. (1995) *Science*, 1754−1758.
48. Zhang, Z. Y., and Dixon, J. E. (1993) *Biochemistry 32*, 9340−9345.
49. Peters, G. H., Frimurer, T. M., and Olson, O. H. (1998) *Biochemistry 37*, 5383−5393.
50. Alhambra, C., Wu, L., Zhang, Z.-Y., and Gao, J. (1998) *J. Am. Chem. Soc. 120*, 3858−3866.
51. Zhang, Z.-Y., Palfey, B. A., Wu, L., and Zhao, Y. (1995) *Biochemistry 34*, 16389−16396.
52. Zhang, Y.-L., Keng, Y.-F., Zhao, Y., Wu, L., and Zhang, Z.-Y. (1998) *J. Biol. Chem. 273*, 12281−12287.
53. Barford, D., Flint, A. J., and Tonks, N. K. (1994) *Science*, 1397−1404.

BI981481Q